Journal of
Nanoscience and Nanotechnology
Vol. 6, 1–5, 2006

Growth of Aligned ZnO Nanorods

A. K. Pradhan,[1,*] T. M. Williams,[1] K. Zhang,[1] D. Hunter,[1] J. B. Dadson,[1]
K. Lord,[1] U. N. Roy,[2] Y. Cui,[2] and A. Burger[2]

[1] *Center for Materials Research, Norfolk State University, Norfolk, VA 23504, USA*
[2] *Department of Physics, Fisk University, 1000, Nashville, TN 37208, USA*

Growth of high-density and aligned ZnO nanorods on ZnO film substrate has been demonstrated using vapor-transport of thermally evaporated Zn metal powders followed by condensation. Morphological studies show that the nanorods grow preferentially from a hexagonal ZnO base with a uniform hexagonal structure following three-dimensional island-like growth mechanism. Structural and spectroscopic properties clearly indicate that the nanorods are relatively good and defect-free in quality. These nanorods have potential for technological implications.

Keywords:

1. INTRODUCTION

Semiconductor nanostructures have attracted intense interest as potential candidates for future electro-optic devices. Among the wide variety of semiconductor nanostructures, ZnO nanostructures are very attractive for high-efficiency short-wavelength optoelectronic nanodevices[1–3] owing to their wide band-gap (3.37 eV) with large excitonic binding energy (≈60 meV), high mechanical and thermal stabilities, transparent conductivity and piezoelectricity. In addition, ZnO nanostructures are believed to be a potential candidate for sensor biological applications. Various one–dimensional (1D) ZnO nanostructures, such as tetrapod nanorods,[4,5] nanowires,[6,7] and nanobelts[8,9] have been reported using various growth methods. However, it is still a significant challenge to obtain controllable growth of ordered nanorods for specific device applications, such as in plastic solar cells,[10] nanolasers,[11] optical storage, nanoscale heterojunctions, etc. Various methods have been utilized to grow ZnO nanostructures on various substrates using catalyst. It is realized that the most useful application may follow from the aligned growth of defect-free nanostructures on a structurally compatible substrate. Therefore, it is important to understand the growth mechanism of aligned nanorods in order to control their growth for specific applications.

In this paper, we report the growth of vertically aligned ZnO nanorods on pulsed-laser deposited ZnO epitaxial film-substrates synthesized by transport of the evaporation of pure Zn metal powders followed by subsequent condensation. The length and diameter of nanorods are highly uniform. Nucleation of ZnO nanorods is facilitated by the surface energy between the ZnO substrate and depositing species. The ZnO nanorods exhibit good structural and spectroscopic properties.

2. EXPERIMENTAL DETAILS

Simple physical solid–vapor–solid transport technique was used to grow ZnO nanorods on *c*-axis oriented ZnO film substrates. High-purity (99.999%) zinc metal powders were used as the starting material. The growth process was performed inside a horizontal tube furnace. The zinc powders of about 0.8 gm were placed in a double crystallized alumina boat. The boat was placed at the center of the furnace tube. The *c*-axis oriented epitaxial ZnO films were grown on single crystalline Al_2O_3 (0001) substrates by multi-target pulsed-laser deposition (PLD) technique (KrF excimer, $\lambda = 248$ nm) with a pulse energy density of 1–2 J/cm^2. 300 nm thick ZnO films were deposited at a substrate temperature of 500 °C, keeping oxygen partial pressure of 1 m Torr and the laser repetition rate of 5 Hz. The X-ray diffraction of the ZnO film shows that the film is highly *c*-axis oriented (Fig. 5). The ZnO substrates used in the present studies was 2 cm (length) × 1 cm (width). The atomic force microscopy (AFM) shows the surface morphology of the substrate, containing ZnO grains of about 20 nm in size and it is illustrated in Figure 1(a). For clarity, AFM image of the ZnO film is shown over 0.5×0.5 μm area in Figure 1(b). The ZnO film was kept about 7 to 8 cm down stream of the tube furnace (opposite to the gas flow). The Ar gas was allowed to flow at a rate of 150 sccm from the opposite direction of the ZnO film substrate. The furnace temperature was ramped at a constant rate of 25 °C/min from room temperature to

*Author to whom correspondence should be addressed.

RESEARCH ARTICLE

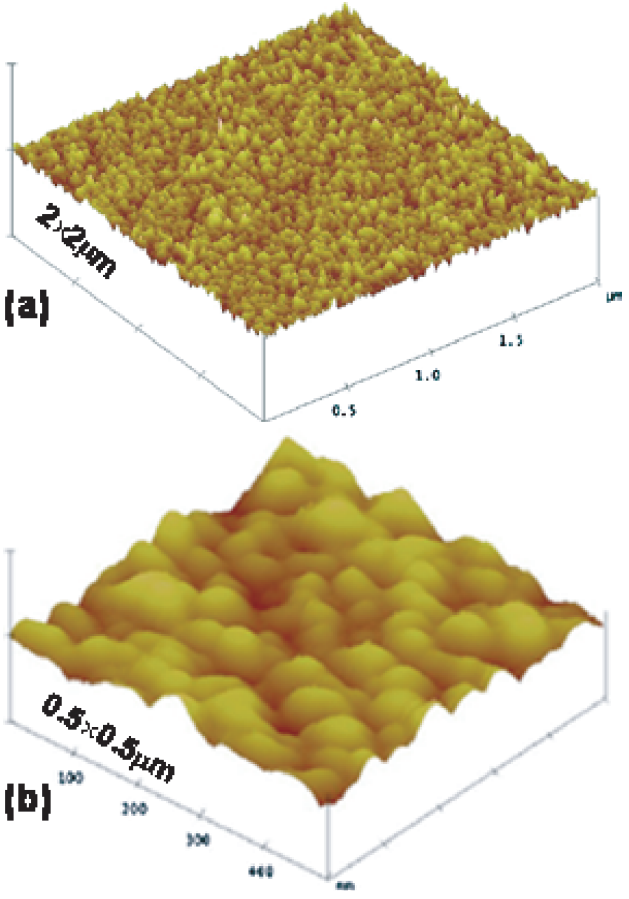

Fig. 1. Atomic force microscopic (AFM) image of ZnO film substrate, (a) over 2×2 μm, and (b) 0.5×0.5 μm area.

760 °C, where the temperature was kept fixed for about 90 min. The zinc powders were vaporized, transported by the carrier Ar gas, and deposited on the substrate. The furnace was cooled after deposition at a rate of 25 °C/min with flowing Ar until the temperature of the furnace reached 400 °C. Then the Ar flow was stopped and one end of the furnace tube was opened to the atmosphere. The ZnO nanorods were formed on the ZnO film substrate.

The films were characterized by X-ray diffraction (XRD) using Rigaku XRD diffractometer (DMAX-3000) equipped with CuK_α radiation. The scanning electron microscopic (SEM) images were taken in a JEOL-SEM microscope. The Raman spectra were recorded in a JY LabRam micro-Raman spectrometer with He-Ne laser excitation at 632.8 nm. The photoluminescence (PL) measurements were carried out at room temperature with a He-Cd laser excited at 325 nm (5 mW of power).

3. RESULTS AND DISCUSSION

The morphology of the as-synthesized ZnO nanostructures shown in Figure 2(a) was seen over a large surface area of the substrate. Vertically aligned ZnO nanorods with well-defined hexagonal flat tops were seen over the region

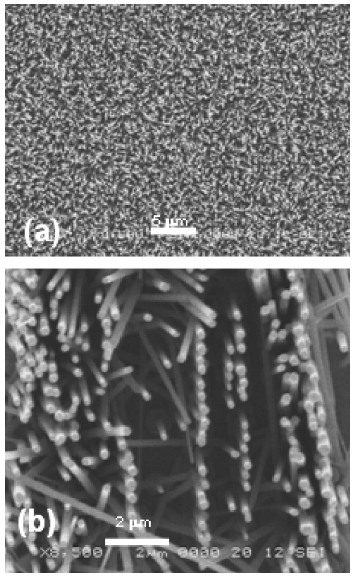

Fig. 2. SEM images of (a) aligned ZnO nanorods (b) aligned ZnO nanorods in a line displaying hexagonal top surface (c).

of the substrate. It is noted that for application in laser emission the flat and smooth top surface is of great interest. The typical dimension of each nanorod is about 60–100 nm wide and 10 to 15 μm long. One of the unique features, such as self-assembly of the nanorods over a long line, is illustrated in Figure 2(b). The hexagonal top surface is very prominent. Some of the nanorods form bundles standing upright with collapsing nanorods from all sides as shown in Figure 3(a). On the other hand, some nanorods align to form fence-like structures (Fig. 3b) although they remain aligned over a long distance.

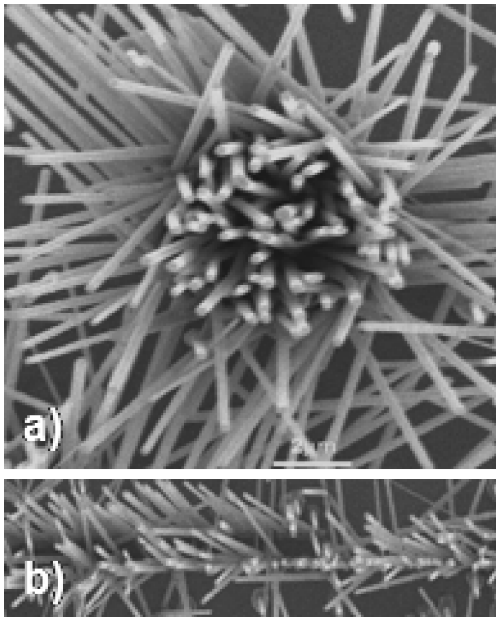

Fig. 3. SEM images of (a) ZnO nanorod bundle showing nanorods falling from the side, and (b) aligned nanorods forming the fence-like structure.

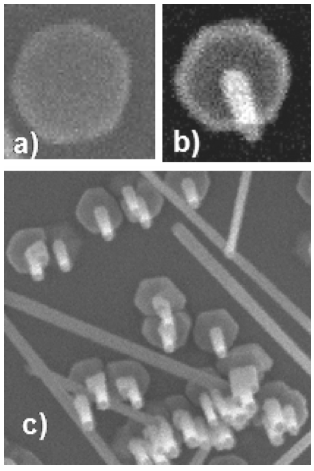

Fig. 4. The growth process was monitored by three different growth times, such as 5, 20, and 30 minutes and their SEM morphology is illustrated in (a) to (c), respectively. SEM images of (a) hexagonal bases, (b) hexagonal bases with sprouting nanorod at the center, and (c) several nanorods from the hexagonal base with similar height and structures are shown.

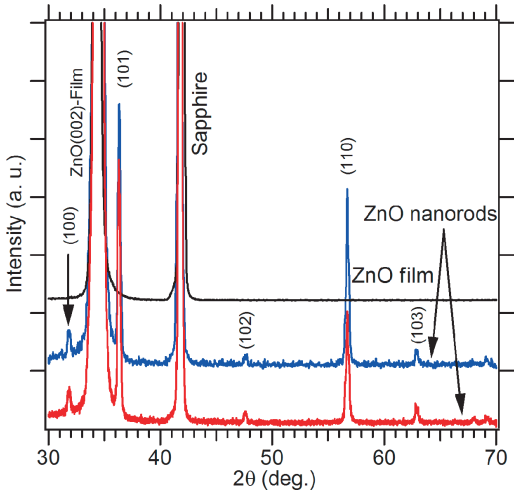

Fig. 5. X-ray diffraction pattern of ZnO nanorods from two positions of the sample and ZnO epitaxial film on $Al_2O_3(0001)$ substrate.

It is important to understand the growth mechanism in order to control the shape, size, and arrangements of nanorods. The morphology studies suggest combination of both layer-by-layer and three-dimensional Volmer-Weber growth mechanism. However, the growth of ZnO nanorods follows two steps and it is described as follows. The growth process was monitored by three different growth times, such as 5, 20, and 30 minutes and their morphology is illustrated Figures 4(a) to (c), respectively. The ZnO nuclei are formed on the lattice matched *c*-axis oriented ZnO substrate maintaining the perfect hexagonal structure and preferentially oriented along the *c*-axis. The orientation and size of the grain domains of the ZnO substrate determine the nucleation site of the first stage of the growth. At first, regular hexagonal array of nucleation sites are formed. In order to support this, a single nucleation site has been imaged and shown in Figure 4(a). The nucleation site is a regular hexagonal base of about 500 nm that corresponds to the (0001) crystal plane of ZnO. The hexagonal bases are very uniform all over the sample. The base hexagonal structures grows both laterally to few hundreds of nm size and in height only a few nm following the layer-by-layer growth mode. However, when the height of the basal plate grows to a certain length in *c*-direction, the nucleation for the growth of the nanorods starts from the center of the base as shown in Figure 4(b). This growth kinetics is followed by the three-dimensional island-like growth as described for Volmer-Weber growth mechanism. The nucleation takes place in all adjacent basal plates at the same time and growth of nanorods occur with the increasing deposition time and shown in Figure 4(c). The increasing deposition time mainly determines the diameter and length of the nanorods, if the temperature of the substrate, gas flow and the distance from the evaporating Zn metal are critically optimized. Well-aligned nanorods are formed when the hexagonal bases are equally placed in a self-assembled way. It is noted that all nanorods have the hexagonal base. All nanorods grow at the same time with equal features and orientations when all other growth conditions are kept constant. The temperature gradient, non-uniform Ar flow and the angle between the direction of metal vapor flow and the substrate can produce different growth arrangements and morphology. Detailed high-resolution microscopy studies are in progress to conform the growth mechanism.

The X-ray diffraction (XRD) patterns of the ZnO substrate and nanorods are displayed in Figure 5. ZnO substrate shows only (0002) peak, illustrating highly *c*-axis oriented epitaxial nature of the film. The XRD pattern of ZnO nanorods recorded at two different positions of the substrates display the typical wurtzite ZnO structure. No diffraction peaks are observed from metallic Zn. The rocking curve of the most intense (0002) diffraction peak with half width at full maxima (FWHM) of the nanorods is about 0.34°, which is close to the FWHM of 0.28 of the ZnO films used for the growth. This clearly signifies that not only the dominating growth direction of the nanorods is the *c*-axis, but also they are of very high crystalline quality. However, other peaks, although less intense, were observed. This is mainly because it is unlikely to have all the nanorods standing upward where the X-ray beam falls on the sample. A slight bending of even a couple of nanorods will show the additional peaks corresponding to the ZnO structure. The observation of only *c*-axis orientation of the aligned nanorods on ZnO substrate in recent XRD report[12] may be either consequence of the diffraction from the substrate or very large ZnO rods of submicron size in diameter as reported. However, our XRD results are consistent with the other reports, such as nanosheets with preferred orientation[13] and aligned nanowires,[14] in which majority of the nanostructures are preferentially aligned in the *c*-direction.

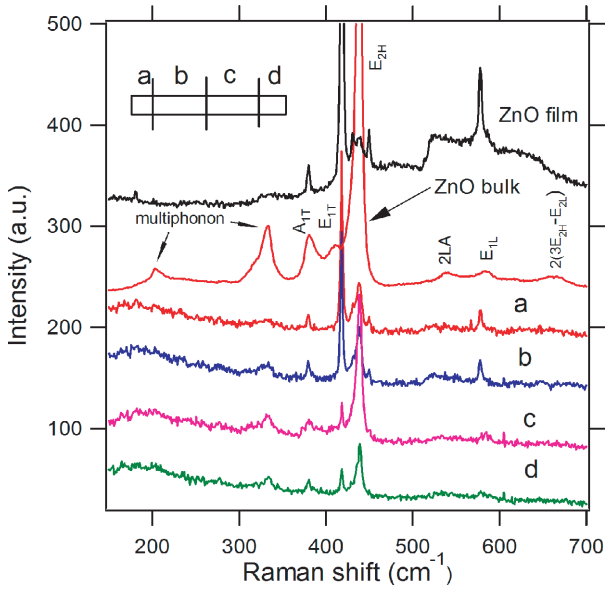

Fig. 6. Raman spectra of ZnO nanorods from different position of the sample as shown in the inset, ZnO film grown on sapphire and ZnO bulk specimen at room temperature. The Raman lines are assigned.

Figure 6 shows the Raman spectra of ZnO film and ZnO nanorods excited with a He-Ne laser at 632.8 nm. The Raman spectrum for ZnO bulk sample is also shown for the comparison. The Raman spectra have been recorded at four different positions of the sample as shown in the inset of Figure 4. All observed Raman peaks are assigned to the wurtzite structure of ZnO as found in the literature.[15, 16] The most remarkable feature in nanorods is the development of E_{2H} peak position at 437 cm^{-1}, which is the most developed peak in ZnO bulk. Figure 4 clearly illustrates that the Raman characteristics of nanorods are almost similar to the ZnO bulk samples, especially in the center region of the film. The E_{2H} phonon frequency at 437 cm^{-1} is generally considered to understand the stress-induced phenomena in wurtzite ZnO nanostructures. An increase in the E_{2H} phonon frequency is ascribed to compressive stress, where as a decrease is due to the tensile stress. This study is advantageous for the qualitative estimation of the residual stress in the nanorods. It is interesting to note that E_{2H} phonon band did not show any shift, illustrating that nanorods are free from stress. However, the overall characteristics of the nanorods are slightly different than those of the ZnO film on sapphire substrate, in which contributions from the strain developed between the film and the substrate, and sapphire substrate are present. On the other hand, the E_1(LO) mode 581 cm^{-1} is caused by the defect due to O-vacancy, Zn-interstitial defect states, or these complexes and free carriers. It is interesting to note that the E_1(LO) phonon mode in nanorods is sharper compared to their bulk counterpart. In view of the above, the Raman spectra clearly elucidate that the ZnO nanorods are of high quality, almost free from defects and strains.

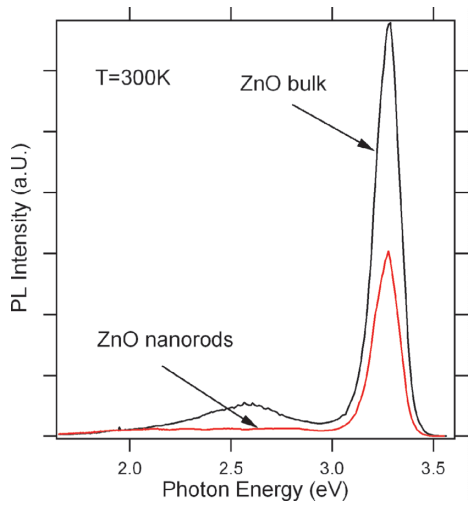

Fig. 7. PL spectra of ZnO nanorods and bulk at room temperature.

Figure 7 represents the photoluminescence (PL) spectra of ZnO nanorods measured at room temperature. The room temperature PL spectrum of the ZnO bulk is shown for the comparison. The PL spectrum of the nanorods shows one dominant emission peak at 3.28 eV and very weak and broad peak at around 2.7 eV. On the contrary, ZnO bulk shows two emission peaks, a dominant peak at about 3.28 eV and broad peak at around 2.62 eV. This signifies two facts that there is no quantum confinement in the nanorods due to their size effects (too large) and, however significant reduction in defects was observed. The observed emission peak at around 2.6 eV in bulk is generally attributed due to the structural defects, such as oxygen defects, dislocations, and also surface defects. The observation of a weak emission peak at about 2.6 eV photon energy regions clearly demonstrates that the present ZnO nanorods are relatively good structural and optical quality compared to many of the ZnO nanostructures in the literatures.[17–19] However, there may be contribution from the surface effects to the PL spectra of nanorods at about 2.6 eV, which cannot be completely ruled out. It is not noted that the most frequently reported deep level band in ZnO are the well known green and yellow-orange bands. It is possible that the band at about 2.6 eV is broad enough to include these components. Although, spectroscopic studies alone cannot confirm the high-quality of the materials alone, further high-resolution microscopic studies are necessary to explore local structural defects.

The catalyst-free growth of ZnO nanorods on ZnO substrate provides unique opportunity to produce highly oriented nanorods, which are relatively free from defects. This technique is superior to catalyst-assisted vapor-liquid-solid (VLS) technique, in which impurity from the catalyst is introduced during the condensation process. Similar growth process for the aligned ZnO nanorods has been reported recently.[20] The high-density self-assembled nanorods on ZnO films have potential applications in photonic and electronic devices. Although the aligned ZnO

RESEARCH ARTICLE

nanorods on ZnO are potential candidate many photonic and electronic applications, the harvested nanorods can be used for nanoscale field-effect-transistors (FET) with electron lithography, biological sensors, and in many new device applications.

4. SUMMARY

In summary, we have grown high-density and aligned ZnO nanorods on ZnO film substrate using vapor-transport of thermally evaporated Zn metal powders. Structural, microscopic, and spectroscopic methods are used to characterize the ZnO nanorods. The growth mechanism for the aligned growth of ZnO nanorods on ZnO film substrate has been elucidated. The nanorods grow preferentially from a hexagonal ZnO base following three-dimensional island-like growth mechanism. Structural and spectroscopic properties indicate that the nanorods are relatively good and defect-free in quality.

Acknowledgments: This work was supported by the NASA Foundation for Center for Research Excellence in Science and Technology via HRD-9805059.

References and Notes

1. M. H. Huang, S. Mao, H. Feick, H. Yan, Y. Wu, H. Kind, E. Weber, R. Russo, and P. Yang, *Science* 292, 1897 **(2001)**.
2. C. J. Lee, T. J. Lee, S. C. Lyu, Y. Zhang, H. Yuh, and H. Lee, *Appl. Phys. Lett.* 81, 3648 **(2002)**.
3. S. C. Jain, M. Willander, J. Narayan, and R. Van Overstraeten, *J. Appl. Phys.* 87, 965 **(2000)**.
4. C. C. Tang, S. S. Fan, M. L. de la Chapelle, and P. Li, *Chem. Phys. Lett.* 333, 12 **(2001)**.
5. Y. Dai, Y. Zhang, Q. K. Li, and C. W. Nan, *Chem. Phys. Lett.* 358, 83 **(2002)**.
6. K. Park, J. S. Lee, M. Y. Sung, and S. Kim, *Jpn. J. Appl. Phys. Part I* 41, 7317 **(2002)**.
7. M. H. Huang, Y. Wu, H. Feick, N. Tran, E. Weber, and P. Yang, *Adv. Mater.* 13, 113 **(2001)**.
8. M. Shiraj, K. Igeta, and M. Arai, *J. Phys. Chem.* 105, 7211 **(2001)**.
9. J. Zhang, W. Yu, and L. Zhang, *Phys. Lett. A* 299, 276 **(2002)**.
10. K. Hara, *Sol. Energy Mater. Sol. Cells* 64, 115 **(2000)**.
11. H. Yumoto, T. Inoue, S. J. Li, T. Sako, and K. Nishiyama, *Thin Sol. Films* 348, 38 **(1999)**.
12. J. Jie, G. Wang, Y. Chen, X. Han, Q. Wang, B. Xu, and J. G. Hou, *Appl. Phys. Lett.* 86, 031909 **(2005)**.
13. S. Chen, Y. Liu, C. Shao, R. Mu, Y. Lu, J. Zhang, D. Shen, and X. Fan, *Adv. Mater.* 17, 586 **(2005)**.
14. L. Wang, X. Zhang, S. Zhao, Y. Zhou, and J. Qi, *Appl. Phys. Lett.* 86, 024108 **(2005)**.
15. M. H. Huang, S. Mao, H. Feick, H. Yan, Y. Wu, H. Kind, E. Weber, R. Russo, and P. Yang, *Science* 292, 1897 **(2001)**.
16. T. C. Damen, S. P. S. Porto, and B. Tell, *Phys. Rev.* 142, 570 **(1966)**.
17. V. A. L. Roy, A. B. Djurisic, W. K. Chan, J. Gao, H. F. Lui, and C. Surya, *Appl. Phys. Lett.* 83, 141 **(2003)**.
18. W. D. Yu, X. M. Li, and X. D. Gao, *Appl. Phys. Lett.* 84, 2658 **(2003)**.
19. J. Q. Hu, Y. Bando, J. H. Zhan, Y. B. Li, and T. Sekiguchi, *Appl. Phys. Lett.* 83, 4414 **(2003)**.
20. Y. Zhang, R. E. Russo, and S. S. Mao, *Appl. Phys. Lett.* 87, 133115 **(2005)**.

Received: 6 January 2006. Revised/Accepted: 15 February 2006.